Transition from nonradiative to radiative oscillons in parametrically driven systems

Alejandro J. Alvarez-Socorro,[1,2] Ernesto Berríos-Caro,[3] Marcel G. Clerc,[1] and Alejandro O. Leon[4,*]

[1]*Departamento de Física and Millennium Institute for Research in Optics, Facultad de Ciencias Físicas y Matemáticas, Universidad de Chile, Casilla 487-3, Santiago, Chile*

[2]*Laboratorio de Investigación, Desarrollo e Innovación, Zenta Group, Andrés Bello 2687, Las Condes, Santiago 7550611, Chile*

[3]*Theoretical Physics, Department of Physics and Astronomy, School of Natural Sciences, Faculty of Science and Engineering, The University of Manchester, Manchester M13 9PL, United Kingdom*

[4]*Instituto de Física, Pontificia Universidad Católica de Valparaíso, Casilla 4059, Chile*

(Received 25 September 2019; revised manuscript received 12 April 2020; accepted 21 April 2020; published 12 May 2020)

Nonequilibrium systems exhibit particle-type solutions. Oscillons are one of the best-known localized states of systems with time-dependent forcing or parametrically driven systems. We investigate the transition from nonradiative to radiative oscillons in the parametrically driven sine-Gordon model in two spatial dimensions. The bifurcation takes place when the strength of the forcing (frequency) increases (decreases) above a certain threshold. As a result of this transition, the oscillon emits radially symmetric evanescent waves. Numerically, we provide the phase diagram and show the supercritical nature of this transition. For small oscillations, based on the amplitude equation approach, the sine-Gordon equation with time-dependent forcing is transformed into the parametrically driven damped nonlinear Schrödinger model in two spatial dimensions. This amplitude equation exhibits a transition between nonradiative to radiative localized structures, consistently. Both models show quite good agreement.

DOI: 10.1103/PhysRevE.101.052209

I. INTRODUCTION

The emergence of complex dynamics on nonequilibrium systems is usually understood as a sequence of bifurcations from a relatively elemental state. For example, a uniform equilibrium can suffer a spontaneous symmetry-breaking instability that generates a pattern structure when the injection of energy is above a threshold [1,2]. When incrementing further the energy injection, the pattern can undergo other bifurcations, leading to phase instabilities [3–6], pulse propagation [4,7], spatiotemporally chaotic states [8,9], among others. The systematic study of secondary instabilities of out-of-equilibrium systems with two or more spatial dimensions remains an open problem.

A compelling case in which nonequilibrium phenomena can appear is the so-called *parametrically driven systems* [10], that is, systems excited by an external force that depends on both time and the state variable of the system. A simple example of parametrically driven systems is a dissipative pendulum whose suspension point oscillates vertically. The pendulum exhibits a parametric resonance as the strength and frequency of the forcing are modified [10]. The dynamical response of a chain of vertically driven damped pendula goes beyond the resonance to include bifurcations that create and stabilize uniform states, Faraday-type bifurcations that induce patterns [11,12], kinks [13,14], and the formation of localized structures [15–17]. Note that these types of solutions are attractors. Namely, under small disturbances, the system converges to the undisturbed state after a transient. Localized states, also known as dissipative solitons, require as a prerequisite a stable background and the capacity to self-focus the energy of the system. Within a range of parameter values, parametrically driven systems satisfy the previous requirements as the energy is relatively modest in the region where the dynamical variable is small (i.e., stable background), and it can be significant where the dynamical variable is large enough. Localized states in two-dimensional (2D) parametrically driven systems have been observed experimentally in various fluids such as fluidized granular media [18], Newtonian [19], and colloidal [20]. Theoretically, the existence and stability properties of nonradiative 2D and 3D oscillations have been studied in the context of parametric driven nonlinear equations [21]. Usually, these solutions are called *oscillons*. Figure 1 illustrates an oscillon in two spatial dimensions. The bi- and one-dimensional profiles of the localized state are shown in Figs. 1(a) and 1(b), respectively. The formation and interaction of oscillons have been the subject of several theoretical, numerical, and experimental studies. However, the dynamical behavior that emerges at the onset of the bifurcations of oscillons has not been fully characterized. In the case of one-dimensional parametrically driven systems, a transition from a localized structure to a breathing localized state, or breather, has been reported [22–25]. Recently, an oscillatory instability of parametrically driven dissipative solitons was numerically studied in magnetic systems in two spatial dimensions [26]. This bifurcation produces highly anisotropic spin waves from the dissipative soliton centroid. Unfortunately, the large amplitude of this localized state rendered the analytic study of this system an arduous task [26].

*alejandro.leon@pucv.cl

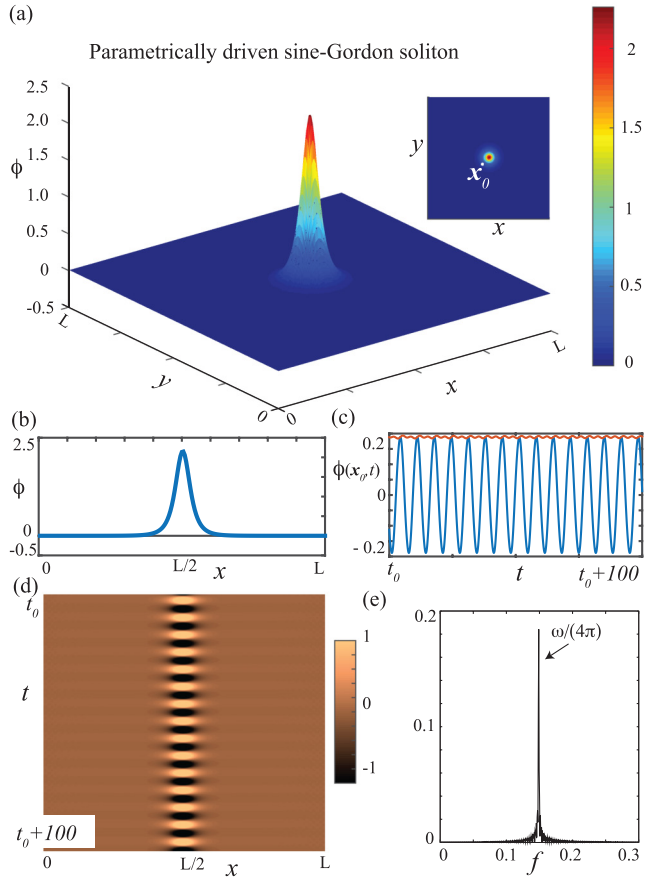

FIG. 1. Nonradiative oscillon of the two-dimensional parametrically driven damped sine-Gordon equation (1) for $\gamma = 0.232$ and $\omega = 1.87$. (a) The oscillon is a self-focused localized state that asymptotically connects to the background solution $\phi = 0$. The origin of the coordinate system is in one of the sample corners, and the lateral size $L = 100$ is divided into 200 points with a spacing of $dx = 0.5$. (b) A one-dimensional cut of (a) shows that the oscillon profile decays monotonically from its center. (c) Temporal evolution of the field $\phi(t, \mathbf{x_0})$, where $\mathbf{x_0} = 0.45L(\hat{\mathbf{x}} + \hat{\mathbf{y}})$. The signal has a dominant frequency, which is nearly half of the forcing frequency. The red curve shows the envelope obtained using the Hilbert transform and the signal $\phi(t, \mathbf{x_0})$. (d) Spatiotemporal diagram of the cut of (a). The color bar is saturated to the range $(-1, 1)$ to emphasize the envelope dynamics. (e) Fourier transform of the trajectory (c) as a function of the frequency f that is equal to 1 divided the period. We observe that the sine-Gordon variable $\phi(t, \mathbf{x_0})$ oscillates at half the forcing frequency $\omega/2 = 1 + \nu$, as expected.

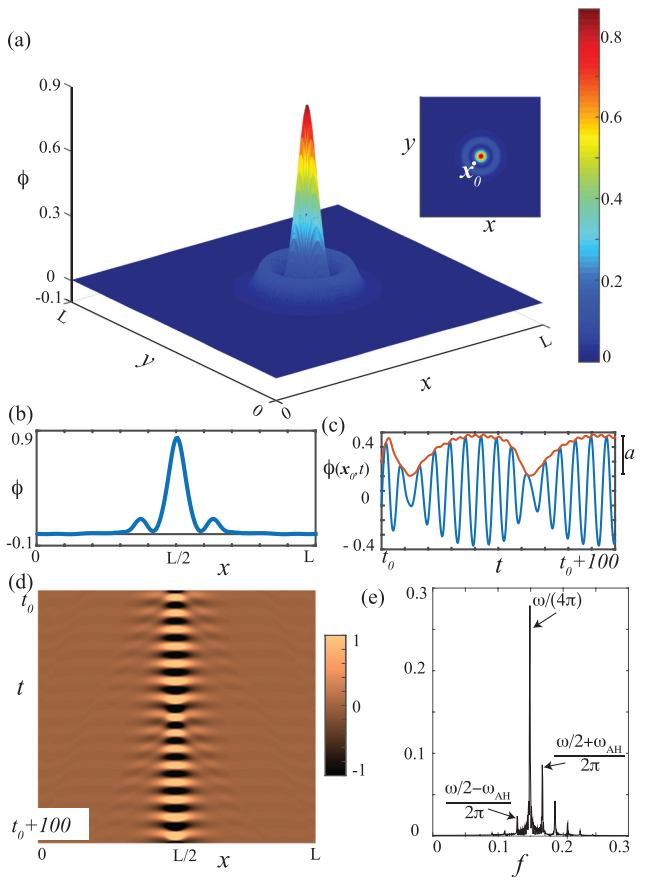

FIG. 2. Radiative oscillon of the two-dimensional parametrically driven damped sine-Gordon equation (1). We plot the same quantities of Fig. 1 for parameter values $\gamma = 0.294$ and $\omega = 1.87$, where γ and ω account for the strength and frequency of the forcing. Panel (c) illustrates the dynamical indicator a, which measures the aperiodicity of the temporal series $\phi(t, \mathbf{x_0})$. Panel (e) shows that in addition to the harmonic oscillation with frequency $\omega/2$, there are Fourier peaks at $\omega/2 \pm n\omega_{\mathrm{AH}}$, with n an integer number. We name ω_{AH} as an *Andronov-Hopf frequency*. For $\gamma = 0.294$ and $\omega = 1.87$, the Andronov-Hopf frequency is $\omega_{\mathrm{AH}} \approx 0.12$. The largest new peak has frequency $\omega/2 + \omega_{\mathrm{AH}}$, which reveals that the envelope of the oscillation of $\phi(t, \mathbf{x_0})$ is modulated in time by an emergent frequency ω_{AH} that is incommensurable with ω.

In this work, we investigate the transition from nonradiative to radiative oscillons in the parametrically driven damped sine-Gordon equation (pdSGE) [27] in two spatial dimensions. Without forcing and dissipation, the two-dimensional sine-Gordon equation admits radial kink solutions with cylindrical symmetry [28–32]. For a small interval of energies of the initial conditions, these kinks can evolve into breatherlike solutions that exhibit periodic oscillations [30]. However, most initial conditions decay into radiation. In the presence of injection and dissipation of energy, the pdSGE can exhibit unusual nonlinear behaviors, such as kinks that emit waves (flaming kinks) [13], decorated interfaces [14], localized structures [33], among others. Here we study the case of *radiative oscillons*, that is, an oscillatory localized spot that emits evanescent waves from its core (see Fig. 2). The evanescent waves are radially symmetric; thus, they have a different phenomenology compared to the one mentioned above of magnetic media (cf. Ref. [26]).

An application of the pdSGE is the description of the phase difference (or flux) ϕ of a long Josephson junction formed by two superconducting films under the influence of an alternating current [27,28]. By long, we mean that its dimensions along the x and y axes are larger than the so-called penetration Josephson depth so that ϕ can vary only in these directions [34]. The penetration depth characterizes the typical penetration of the magnetic field applied to the junction, and it is usually of tens of nanometers [35]. Josephson junctions have been studied for the design of particle detectors [36],

SQUIDs [35], and exponentially tapered Josephson flux-flow oscillators [37,38].

The pdSGE has a simpler mathematical structure compared to the one of the so-called Landau-Lifshitz-Gilbert model that governs magnetic systems [39]. The latter has nonlinear dissipation, linear and nonlinear diffusion and dispersion, among other terms. The relatively simpler form of the pdSGE allows one to apply analytic techniques, such as the amplitude equation formalism, to transform the pdSGE into the well-known parametrically driven damped nonlinear Schrödinger (pdNLS) equation. This change of variables (reviewed later on) eliminates the explicit time dependence and allows us to show that the bifurcation is a supercritical Andronov-Hopf (i.e., oscillatory) instability. Direct numerical simulations of the sine-Gordon equation confirm the results of the pdNLS equation. A numerical phase diagram of the dissipative solitons of the pdSGE is also provided.

The article is organized as follows. In the next section, we introduce the parametrically driven damped sine-Gordon equation and show the oscillon state before and after its oscillatory instability. In Secs. II A and II B, we review the transformation of the pdSGE into the pdNLS one and characterize the phase diagram of the amplitude equation, respectively. Section III presents our conclusions and final remarks.

II. THE SINE-GORDON EQUATION

Let us consider the two-dimensional parametrically driven damped sine-Gordon equation (pdSGE) [27]

$$\partial_{tt}\phi = -[1 + \gamma \sin \omega t] \sin \phi - \mu \partial_t \phi + \nabla^2 \phi, \qquad (1)$$

where $\phi = \phi(t, \mathbf{r})$ is the dynamical variable that depends on time (t) and space ($\mathbf{r} = x\hat{\mathbf{x}} + y\hat{\mathbf{y}}$). The unit vectors $\hat{\mathbf{x}}$ and $\hat{\mathbf{y}}$ point along the x and y Cartesian axes, respectively, and $\nabla^2 = \partial_{xx} + \partial_{yy}$ is the Laplacian operator. The dimensionless parameters μ and $\{\gamma, \omega\}$ account for the energy dissipation and the strength and frequency of the forcing, respectively. In the following, we fix the dissipation coefficient to $\mu = 0.1$. We do not consider the dispersion and natural frequency as varying parameters since the time and spatial coordinates can always be renormalized to make them equal to 1, as we have done. The parametric resonance regime begins when the forcing frequency is about twice the natural one, i.e., $\omega = 2(1 + \nu)$, where the parameter ν is a small detuning. For large enough injections of energy, the system exhibits patterns formation [11,12] for $\nu > 0$ and localized structures [15–17] for $\nu < 0$. Figure 1 shows the typical localized state observed in the pdSGE. These localized solutions are bell-shaped in the magnitude of the amplitude and constant in the phase for periodic boundary conditions. However, for Neumann boundary conditions, the oscillations may have a complex phase structure (e.g., phase shielding solitons [40,41]). Despite the apparent simplicity of the oscillons with a homogeneous phase, they do not have a known analytical expression.

We integrate Eq. (1) in a square simulation box of size $L \times L$ using a Runge-Kutta algorithm, as detailed in Appendix. For Fig. 1, we used $\gamma = 0.232$ and $\omega = 1.87$. The three-dimensional representation of the oscillon in Fig. 1(a) accounts for a localized peak in the angle ϕ that is symmetric around its center or centroid. Figure 1(b) illustrates the oscillon profile that is a monotonically decaying function of the radial distance from its centroid. This figure was made for a time in which the forcing value is maximum. A simple indicator of the dynamics of the oscillon is the temporal evolution of a single and arbitrary point of it, $\mathbf{x_0}$. We used $\mathbf{x_0} = 0.45L(\hat{\mathbf{x}} + \hat{\mathbf{y}})$, and Fig. 1(c) shows the time evolution of $\phi(t, \mathbf{x_0})$. This graph reveals a single frequency and an almost constant oscillation envelope [cf. the Fourier transform of $\phi(t, \mathbf{x_0})$ in Fig. 1(e)]. The envelope is calculated via the built-in Hilbert transform of MATLAB software. The nonlinear corrections of the (mainly) harmonic signal $\phi(t, \mathbf{x_0})$ manifest as a small oscillation in the envelope. The difference between the maximum and minimum values of the temporal series of the envelope provides a single number for each pair (ω, γ) parameter value: $a(\omega, \gamma)$. Likewise, to illustrate the oscillatory nature of oscillons, one can analyze the temporal evolution of a solution cut [see Fig. 1(d)]. This way, all the points of the localized state oscillate in solidarity.

When the forcing amplitude is increased (or the forcing frequency is decreased), the oscillon undergoes an oscillatory instability that generates radial emission of evanescent waves from its center. Figure 2 shows this dynamical behavior for $\gamma = 0.294$ and $\omega = 1.87$. The top view snapshot of the oscillon shows a structure of rings around its center [see Fig. 2(a)], which breaks the monotonic decay of its envelope, as shown in Fig. 2(b). As in Fig. 1(b), these images were also taken at times in which the strength of the forcing is maximum. Notice that the presence of the evanescent wave from the oscillon core modifies the temporal evolution of the field $\phi(t, \mathbf{r})$. For example, in $\mathbf{x_0}$, the trajectory $\phi(t, \mathbf{x_0})$ of Fig. 2(c) is similar to that of Fig. 1(c) with an additional modulation of the envelope, which is a manifestation of the evanescent wave. Figure 2(d) shows a spatiotemporal diagram of a cut of the oscillon, illustrating the emission of evanescent waves from its core. Numerically, we have tested that the evanescent wave speed corresponds to nonlinear (linear) waves near (far from) the centroid. Namely, the evanescent waves satisfy the dispersion relation given by small-amplitude perturbations around $\phi = 0$ only outside the ringlike structure that surrounds the localized state. Figure 2(e) shows $\phi(t, \mathbf{x_0})$ in frequency space. The spectrum has peaks at frequencies $\omega/2 \pm n\omega_{\mathrm{AH}}$, with n an integer number. The additional Andronov-Hopf frequency, ω_{AH}, is not commensurable with ω nor with ν, which allows us to conjecture that it is the result of an instability of the oscillon envelope. Hence, the dynamics in the flanks of the oscillon are characterized by exhibiting quasiperiodic dynamical behavior.

To quantify the transition from nonradiative to radiative oscillons, we use the oscillation amplitude of the envelope of the temporal series $\phi(t, \mathbf{x_0})$, namely $a(\omega, \gamma)$. This is a useful dynamical indicator that plays the role of an order parameter. Furthermore, since it measures the amplitude of the quasiperiodic part of $\phi(t, \mathbf{x_0})$, it is approximately the Fourier amplitude of the frequency $\omega/2 + \omega_{\mathrm{AH}}$. Figure 3(a) shows the bifurcation diagram of the system for $\omega = 1.88$. The oscillon emerges for $\gamma_{c1} = 0.223$ by a saddle-node bifurcation and undergoes an instability at $\gamma_{c2} \approx 0.251$. In this region, the wave amplitude [proportional to $a(\omega, \gamma)$] grows continuously, which is a characteristic of the supercritical bifurcations [1,2]. The thick dots of Fig. 3 are the results of the numerical simulation, while the solid curve of Fig. 3(a) is the curve fitting

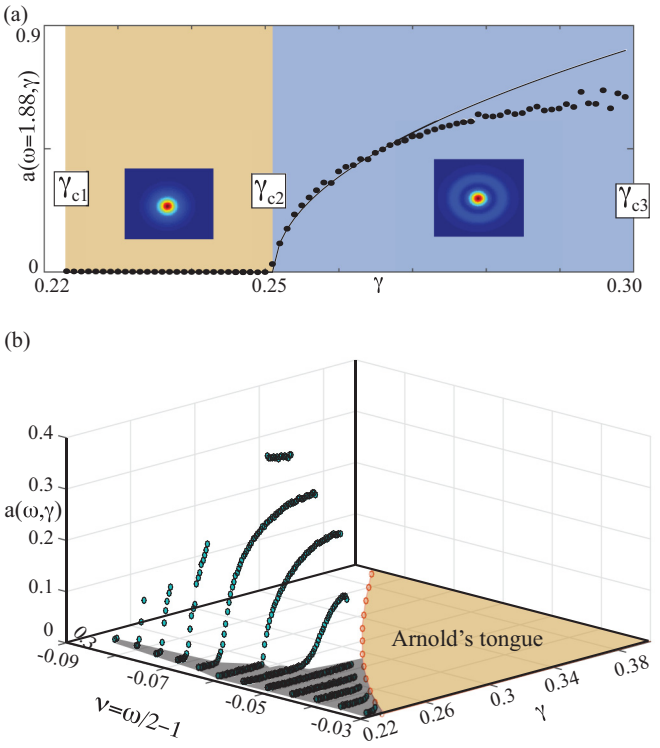

FIG. 3. Bifurcation diagram of the two-dimensional parametrically driven damped sine-Gordon equation (1). (a) The oscillation amplitude of the envelope of the temporal series $\phi(t, \mathbf{x_0})$ with $\mathbf{x_0} = 0.45L(\hat{\mathbf{x}} + \hat{\mathbf{y}})$ is plotted for $\omega = 1.88$. This diagram shows the supercritical transition from nonradiative to radiative oscillons. Thick dots account for the simulation results, while the solid line for the curve fitting $a(\omega = 1.88, \gamma) = \sqrt{0.17\gamma - 0.0427}$, where γ and ω account for the strength and frequency of the forcing. (b) Bifurcation diagram in the (ν, γ) plane, where ν is the detuning.

$a(\omega = 1.88, \gamma) = \sqrt{0.17\gamma - 0.0427}$. As γ moves away from the bifurcation point, the amplitude of the evanescent wave begins to move away from the theoretical fitting, which is a manifestation of superior nonlinear effects. The radiative oscillon persists until $\gamma_{c3} = 0.299$, where the 2:1 Arnold's tongue region is reached, and the $\phi = 0$ state becomes unstable. Since the localized state needs a stable background, it disappears for $\gamma > \gamma_{c3}$. Figure 3(b) shows the bifurcation diagram in the (ω, γ) plane. As this plot illustrates, evanescent waves emerge via a supercritical instability for all frequencies. When the forcing frequency is further decreased, the soliton is destabilized, and the field ϕ decays to the $\phi = 0$ state. To elucidate the origin of this transition and characterize its universality, based on weakly nonlinear analysis, we will review the derivation of the envelope equation of the pdSGE and analyze its localized solutions.

A. Parametrically driven damped nonlinear Schrödinger equation

Physical systems at the onset of their resonances and instabilities exhibit a separation of temporal scales [2]. In the case of parametrically driven media, the oscillation phase of the state variables is much faster than the temporal variation of their amplitude, which motivates the use of the so-called *amplitude equation* [2] formalism. The derivation of the pdNLS model from the sine-Gordon equations is known for one-dimensional [17,42] and two-dimensional systems [21]. Let us review the derivation by replacing the following ansatz in Eq. (1):

$$\phi(t, \mathbf{r}) = A(t, \mathbf{r}')e^{i(1+\nu)t} + W(A, \bar{A}) + \text{c.c.}, \tag{2}$$

where $A(t, \mathbf{r}')$ is the oscillation envelope with $\mathbf{r}' = x'\hat{\mathbf{x}} + y'\hat{\mathbf{y}} = \sqrt{2}\mathbf{r}$, and c.c. denotes the complex conjugate. The function W represents the correction due to nonlinear terms and depends both on A and its complex conjugate $\bar{A}$. The amplitude A is assumed small, but larger than the nonlinear W, i.e., $|W| \ll |A|$. It is assumed that A is a slow variable, such that its temporal derivatives become even smaller ($|\partial_{tt}A| \ll |\partial_t A| \ll |A|$). One also considers the scaling $|A|^2 \sim \mu \sim |\nu| \sim \gamma \sim |\partial_t A|/|A| \ll 1$. Note that the change of variables (2) is general for parametrically driven systems near the 2:1 resonance.

By setting $\omega = 2(1 + \nu)$ with small detuning, $|\nu| \ll 1$, i.e., close to twice the natural frequency, and regrouping the dominant terms when replacing the ansatz into Eq. (1), one gets a linear system in W. Applying solvability conditions [2] yields

$$\partial_t A = -i\nu A - \frac{i}{4}A|A|^2 - \frac{\mu}{2}A + \frac{\gamma}{4}\bar{A} - i\nabla'^2 A, \tag{3}$$

with ∇'^2 the Laplacian with respect to the spatial variable $\mathbf{r}'$. The above equation has been derived in several physical contexts to describe patterns and localized structures such as vertically oscillating layers of water [15], nonlinear lattices [43], optical fibers [44], Kerr-type optical parametric oscillators [45], and magnetization in an easy-plane ferromagnetic exposed to an oscillatory magnetic field [17].

B. Characterization of the dynamics of the pdNLS equation

Let us start by reviewing some known solutions of the pdNLS equation and their corresponding stability. Equation (3) allows us to determine the stability regions of the quiescent state $A = 0$ with a simple linear analysis [46]. For that, one decomposes A into its real and imaginary parts, $A = u + iv$, and linearizes on them to get [46]

$$\frac{d}{dt}\begin{pmatrix} u \\ v \end{pmatrix} = \begin{bmatrix} \gamma/4 - \mu/2 & \nu + \nabla'^2 \\ -(\nu + \nabla'^2) & -\gamma/4 - \mu/2 \end{bmatrix}\begin{pmatrix} u \\ v \end{pmatrix}. \tag{4}$$

The eigenvalues of the above equation are $\lambda_\pm(\mathbf{k}) = -\mu/2 \pm \sqrt{\gamma^2/16 - (\nu - k^2)^2}$, where $\mathbf{k}$ is the wave vector of the perturbation with norm $|\mathbf{k}| = k$. The stability condition is $\lambda_\pm(\mathbf{k}) < 0$ for all $\mathbf{k}$. The stability analysis of this equation is well known, and it reveals that there is a region in the (γ, ν) plane bounded by the curve $\mu^2 + 4\nu^2 = \gamma^2/4$, where $A = 0$ becomes unstable against uniform perturbations [46]. In the context of parametrically forced systems, this region is usually referred to as 2:1 *Arnold's tongue*, as it is located around twice the natural frequency. Figure 4(b) shows the 2:1 Arnold's tongue in the phase diagram. Spacial instabilities occur for $\nu > 0$ [12], where oscillons do not exist. Thus, the spacial instability is not considered here.

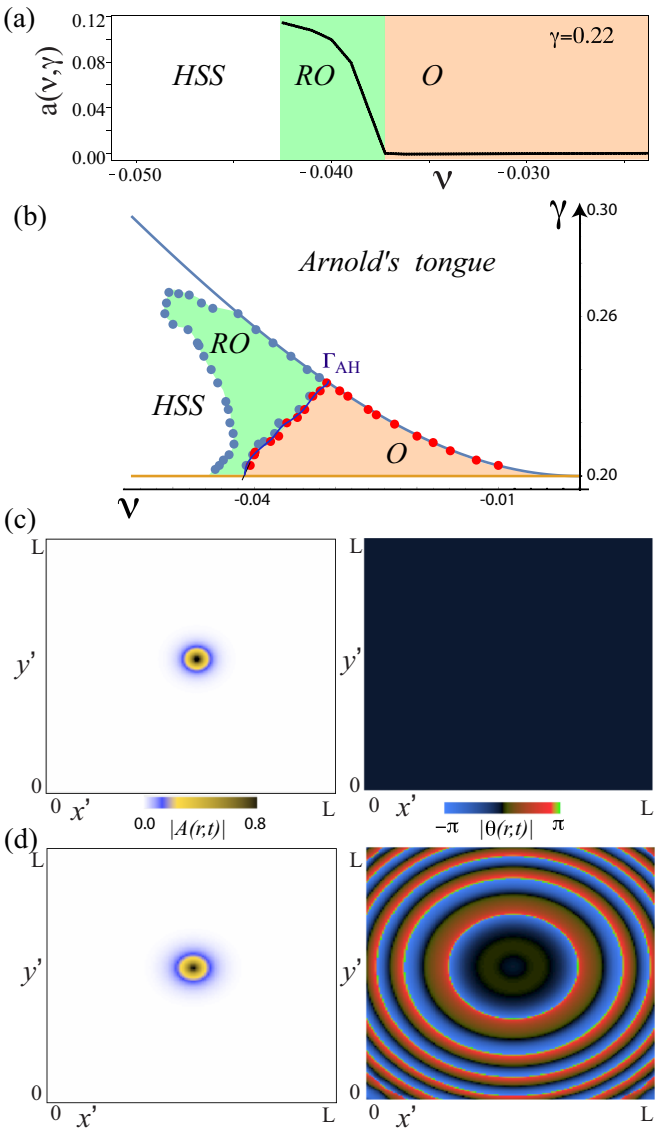

FIG. 4. Radiative and nonradiative oscillons of the parametrically driven damped nonlinear Schrödinger Eq. (3) with $\mu = 0.1$. (a) Bifurcation diagram of the pdNLS model for $\gamma = 0.22$. Vertical amplitude oscillation $a(\nu, \gamma)$ in a given point as a function of the detuning. (b) Phase diagram of the pdNLS equation. This plot shows the supercritical nature of the instability. The regions O, RO, and HSS account for the zones of the parameter space where the nonradiative oscillons, radiative oscillons, and uniform homogeneous steady state are observed, respectively. $\Gamma_{\rm AH}$ is the transition curve from nonradiative to radiative oscillons. (c) Snapshot of a nonradiative oscillon for detuning $\nu = -0.025$, forcing strength $\gamma = 0.208$, and $L = 200 \times 0.7$. The left and right panel account for the modulus and phase of the amplitude, respectively. The simulation box has 200×200 points and spatial step size $dx = 0.7$. (d) Snapshot of a radiative oscillon for $\nu = -0.42$ and $\gamma = 0.216$.

For forcing frequencies close to the 2:1 resonance (i.e., $|\nu| \ll 1$) and $\mu \lesssim \gamma$, the amplitude Eq. (3) exhibits bell-shaped amplitude solutions with a homogeneous phase [21,47]. These localized states account for oscillons of the oscillatory driven system. Figure 4 shows the region of parameters where the nonradiative (O) and radiative (RO) oscillations are observed. It is important to note that analytical solutions for the oscillons are not known in two spatial dimensions. The existence and stability zones of the two- and three-dimensional nonradiative oscillons were studied in Ref. [21] in the injection-dissipation (γ-μ, μ) plane. In particular, it is analytically established that the oscillon suffers an oscillatory instability. Here we focus on the transition that occurs for negative detuning when its modulus is large enough to induce radiation from the oscillon core, i.e., a *radiative oscillon* (cf. Fig. 4). When one begins from the region where oscillons are observed and decreases the forcing strength γ, the localized spot becomes unstable through a saddle-node bifurcation for $\gamma = \mu$. This condition is represented by the horizontal curve in Fig. 4(b), and it has been studied analytically for one- [17], two-, and three-dimensional solitons [21] for the pdNLS model. The previous scenario changes when one decreases the modulus of the detuning parameter, $\nu \to 0$. When crossing the 2:1 Arnold's tongue, the localized spot becomes unstable and is replaced by a square pattern. This bifurcation of the oscillons originates from the loss of stability of the support state $A = 0$ [46] to which to soliton asymptotically connects.

When one decreases the detuning, the oscillation becomes unstable via a supercritical oscillatory instability (Andronov-Hopf). The transition curve from nonradiative to radiative oscillons in the parameter space is represented by $\Gamma_{\rm AH}$ in Fig. 4(b). This transition creates radiative oscillons. Figure 4(c) shows the typical magnitude and phase of the radiative oscillon in a given time. Decreasing further the detuning parameter, radiative oscillons become unstable by means of a saddle-node bifurcation. This scenario changes for large γ parameter and negative detuning, close to the 2:1 Arnold's tongue, where radiative oscillons become unstable by giving rise to localized solutions with complex spatiotemporal behaviors. The study of such structures has not been reported and remains an open problem.

III. CONCLUSIONS

The instabilities of spatiotemporal states, such as two-dimensional patterns and localized structures, are not fully understood. In this work, we studied the oscillatory bifurcation of oscillons in the two-dimensional parametrically driven sine-Gordon equation. We studied the transition from nonradiative to radiative oscillons in the oscillation envelope representation and found an Andronov-Hopf bifurcation. Direct numerical simulation of the sine-Gordon equation confirmed this scenario. The bifurcation diagram of the system, in the frequency-forcing amplitude plane, was also provided.

ACKNOWLEDGMENTS

We gratefully acknowledge financial support in Chile from Becas Conicyt 2015 Contract No. 21151618, Postdoctorado FONDECYT 2019 Folio 3190030, Financiamento Basal para Centros Cientificos de Excelencia FB0807, and the Millennium Institute for Research in Optics (Miro). We acknowledge support through a Presidential Doctoral Scholarship (The University of Manchester) to EBC.

APPENDIX: NUMERICAL METHODS

We solve the parametrically driven sine-Gordon equation by dividing the space into 200×200 points separated by a distance of $dx = 0.5$. The Laplacian $\nabla^2\phi$ is approximated using a centered scheme [48] of order 6. The time is also discretized with step size $dt = 0.05$ and the field $\phi(t + dt, \mathbf{r})$ is obtained from $\phi(t, \mathbf{r})$ with a fifth-order Runge-Kutta algorithm [49]. For every solution of Figs. 1, 2, and 3(a), an initial condition was integrated in 244 000 iterations, which is long enough to guarantee that the system converges to one of its stationary states.

The bifurcation diagrams are obtained via the so-called *continuation method*. In this scheme, the final state of a simulation of ϕ for parameters (ω_1, γ_1) is the initial condition for (ω_2, γ_2), such that $|\omega_1 - \omega_2| \ll \omega_1$ and $|\gamma_1 - \gamma_2| \ll \gamma_1$. We started with a soliton state for $\omega = 1.88$ and $\gamma = 0.295$ and moved the values of γ with a step size of $d\gamma = 0.001$ to make Fig. 3(a). Then for every value of γ at $\omega = 1.88$, the frequency is varied with a step size of $d\omega = 0.01$. Once the temporal series are obtained, we use the dynamical indicator a introduced earlier to distinguish between a nonradiative and radiative oscillon. In the former case, the nonradiative oscillon has an almost constant temporal Hilbert transform, while in the latter, the envelope has significant differences [cf. Figs. 1(c) and 2(c)]. The results are plotted in Fig. 3(b). Note that ϕ obeys a nonlinear equation, and then the Hilbert transform is never a constant. Thus, in Fig. 3(a) we subtract the minimum of the a values, $a(\omega, \gamma) \to a(\omega, \gamma) - \min_{\omega,\gamma}[a]$.

[1] M. C. Cross and P. C. Hohenberg, Pattern formation outside of equilibrium, Rev. Mod. Phys. **65**, 851 (1993).

[2] L. M. Pismen, *Patterns and Interfaces in Dissipative Dynamics* (Springer, Berlin, 2006).

[3] P. Coullet and G. Iooss, Instabilities of One-Dimensional Cellular Patterns, Phys. Rev. Lett. **64**, 866 (1990).

[4] L. Gil, Instabilities of one-dimensional cellular patterns: Far from the secondary threshold, Europhys. Lett. **48**, 156 (1999).

[5] L. Pan and J. R. de Bruyn, Spatially uniform traveling cellular patterns at a driven interface, Phys. Rev. E **49**, 483 (1994).

[6] P. Coullet, R. E. Golstein, and G. H. Gunaratne, Parity-Breaking Transitions of Modulated Patterns in Hydrodynamic Systems, Phys. Rev. Lett. **63**, 1954 (1989).

[7] A. O. Leon, M. G. Clerc, and S. Coulibaly, Traveling pulse on a periodic background in parametrically driven systems, Phys. Rev. E **91**, 050901 (2015).

[8] M. G. Clerc and N. Verschueren, Quasiperiodicity route to spatiotemporal chaos in one-dimensional pattern-forming systems, Phys. Rev. E **88**, 052916 (2013).

[9] M. G. Clerc, G. González-Cortés, V. Odent, and M. Wilson, Optical textures: characterizing spatiotemporal chaos, Opt. Express **24**, 15478 (2016).

[10] L. D. Landau and E. M. Lifshiftz, *Mechanics*, Course of Theoretical Physics Vol. 1 (Pergamon, Oxford, 1976).

[11] M. Faraday, On a peculiar class of acoustical figures; and on certain forms assumed by groups of particles upon vibrating elastic surfaces, Philos. Trans. R. Soc. London **121**, 299 (1831).

[12] P. Coullet, T. Frisch, and G. Sonnino Dispersion-induced patterns, Phys. Rev. E **49**, 2087 (1994).

[13] E. Berríos-Caro, M. G. Clerc, and A. O. Leon, Flaming 2π-kinks in parametrically driven systems, Phys. Rev. E **94**, 052217 (2016).

[14] E. Berríos-Caro, M. G. Clerc, M. A. Ferre, and A. O. Leon, Oscillating decorated interfaces in parametrically driven systems, Phys. Rev. E **97**, 012207 (2018).

[15] J. W. Miles, Parametrically excited solitary waves, J. Fluid Mech. **148**, 451 (1984).

[16] H. J. Mikeska, Solitons in a one-dimensional magnet with an easy plane, J. Phys. C **11**, L29 (1978).

[17] I. V. Barashenkov, M. M. Bogdan, and V. I Korobov, Stability diagram of the phase-locked solitons in the parametrically driven, damped nonlinear Schrödinger equation, Europhys. Lett. **15**, 113 (1991).

[18] P. B. Umbanhowar, F. Melo, and H. L. Swinney, Localized excitations in a vertically vibrated granular layer, Nature (London) **382**, 793 (1996).

[19] H. Arbell and J. Fineberg, Temporally Harmonic Oscillons in Newtonian Fluids, Phys. Rev. Lett. **85**, 756 (2000).

[20] O. Lioubashevski, Y. Hamiel, A. Agnon, Z. Reches, and J. Fineberg, Oscillons and Propagating Solitary Waves in a Vertically Vibrated Colloidal Suspension, Phys. Rev. Lett. **83**, 3190 (1999).

[21] I. V. Barashenkov, N. V. Alexeeva, and E. V. Zemlyanaya, Two- And Three-Dimensional Oscillons in Nonlinear Faraday Resonance, Phys. Rev. Lett. **89**, 104101 (2002).

[22] N. V. Alexeeva, I. V. Barashenkov, and D. E. Pelinovsky, Dynamics of the parametrically driven NLS solitons beyond the onset of the oscillatory instability, Nonlinearity **12**, 103 (1999).

[23] I. V. Barashenkov and E. V. Zemlyanaya, Soliton complexity in the damped-driven nonlinear Schrödinger equation: Stationary to periodic to quasiperiodic complexes, Phys. Rev. E **83**, 056610 (2011).

[24] I. V. Barashenkov, E. V. Zemlyanaya, and T. C. van Heerden, Time-periodic solitons in a damped-driven nonlinear Schrödinger equation, Phys. Rev. E **83**, 056609 (2011).

[25] D. Urzagasti, D. Laroze, M. G. Clerc, and H. Pleiner, Breather soliton solutions in a parametrically driven magnetic wire, Europhys. Lett. **104**, 40001 (2013).

[26] A. O. Leon, M. G. Clerc, and D. Altbir, Dissipative magnetic breathers induced by time-modulated voltages, Phys. Rev. E **98**, 062213 (2018).

[27] J. C. Eilbeck, P. S. Lomdahl, O. H. Olsen, and M. R. Samuelsen, Comparison between one-dimensional and two-dimensional models for Josephson junctions of overlap type, J. Appl. Phys. **57**, 861 (1985).

[28] J. Cuevas-Maraver, P. G. Kevrekidis, and F. Williams, *The sine-Gordon Model and Its Applications. Nonlinear Systems and Complexity* (Springer, Switzerland, 2014).

[29] P. L. Christiansen and P. S. Lomdahl, Numerical study of 2+1 dimensional sine-Gordon solitons, Physica D **2**, 482 (1981).

[30] J. Geicke, On the reflection of radially symmetrical sine-Gordon kinks in the origin, Phys. Lett. A **98**, 147 (1983).

[31] J. G. Caputo and M. P. Soerensen, Radial sine-Gordon kinks as sources of fast breathers, Phys. Rev. E **88**, 022915 (2013).
[32] J. Geicke, Cylindrical pulsons in nonlinear relativistic wave equations, Phys. Scr. **29**, 431 (1984).
[33] M. A. Ferré, S. Coulibally, R. G. Rojas, and M. Tlidi, Localized structures and spatiotemporal chaos: Comparison between the driven damped sine-Gordon and the Lugiato-Lefever model, Eur. Phys. J. D **71**, 172 (2017).
[34] J. Mazo and A. V. Ustinov, The sine-Gordon equation in Josephson-junction arrays. *The sine-Gordon model and its applications* (Springer, Cham, 2014).
[35] K. K. Likharev, *Dynamics of Josephson Junctions and Circuits* (Gordon and Breach Science, 1986).
[36] S. Pagano, C. Nappi, R. Cristiano, E. Esposito, L. Frunzio, L. Parlato, G. Peluso, G. Pepe, and U. Scott Di Uccio, *Nonlinear Superconducting Devices and High Tc Materials* (World Scientific, Singapore, 1995).
[37] A. Benabdallah, J. G. Caputo, and A. C. Scott, Exponentially tapered Josephson flux-flow oscillator, Phys. Rev. B **54**, 16139 (1996).
[38] A. Benabdallah, J. G. Caputo, and A. C. Scott, Laminar phase flow for an exponentially tapered Josephson oscillator, J. Appl. Phys. **88**, 3527 (2000).
[39] I. D. Mayergoyz, G. Bertotti, and C. Serpico, *Nonlinear Magnetization Dynamics in Nanosystems* (Elsevier, Oxford, 2009).
[40] M. G. Clerc, S. Coulibaly, M. A. Garcia-Nustes, and Y. Zarate, Dissipative Localized States with Shieldlike Phase Structure, Phys. Rev. Lett. **107**, 254102 (2011).
[41] M. G. Clerc, M. A. Garcia-Nustes, Y. Zarate, and S. Coulibaly, Phase shielding soliton in parametrically driven systems, Phys. Rev. E. **87**, 052915 (2013).
[42] N. V. Alexeeva, I. V. Barashenkov, and G. P. Tsironis, Impurity-Induced Stabilization of Solitons in Arrays of Parametrically Driven Nonlinear Oscillators, Phys. Rev. Lett. **84**, 3053 (2000).
[43] B. Denardo B. Galvin, A. Greenfield, A. Larraza, S. Putterman, and W. Wright, Observations of Localized Structures in Nonlinear Lattices: Domain Walls and Kinks, Phys. Rev. Lett. **68**, 1730 (1992).
[44] J. N. Kutz, W. L. Kath, R. D. Li, and P. Kumar, Long-distance pulse propagation in nonlinear optical fibers by using periodically spaced parametric amplifiers, Opt. Lett. **18**, 802 (1993).
[45] S. Longhi, Stable multipulse states in a nonlinear dispersive cavity with parametric gain, Phys. Rev. E **53**, 5520 (1996).
[46] M. G. Clerc, S. Coulibaly, and D. Laroze, Parametrically driven instabilities in quasi-reversal systems, Int. J. Bifurcation Chaos **19**, 3525 (2009).
[47] M. G. Clerc, S. Coulibaly, and D. Laroze, Interaction law of 2D localized precession states, Europhys. Lett. **90**, 38005 (2010).
[48] J. M. Hyman and B. Larrouturou, The numerical differentiation of discrete functions using polynomial interpolation methods, Appl. Math. Comput. **10**, 487 (1982).
[49] W. H. Press, S. A. Teukolsky, W. T. Vetterling, and B. P. Flannery, *Numerical Recipes in C* (Cambridge University Press, Cambridge, 1996), Vol. 2.